# Optimization of an Inverse Convection Solution Strategy

Joseph R VanderVeer, Yogesh Jaluria*

*Department of Mechanical and Aerospace Engineering: Rutgers University, 98 Brett Rd, Piscataway NJ, 08854*

**Abstract**

*Keywords:* Inverse Problems, Computational Heat Transfer, Convection

## 1. Introduction

Thermal-fluid systems often create situations where the engineering problem is an inverse heat transfer problem. These problems often have limited physical access, very limited to no boundary condition knowledge, and/or limited domain knowledge.

For example, the temperature distribution of an optical fiber drawing furnace is difficult to measure directly due to shape, inaccessibility, and high temperatures. The center of the furnace is easily accessible and this directly leads to an inverse heat transfer problem. Issa et al. [1] [1] developed a regularization technique utilizing the centerline temperature from which the wall temperature may be obtained.

Another example, is the inverse plume in a crossflow problem. The problem entails solving for the plume boundary conditions utilizing limited domain knowledge. A novel predictor-corrector method was developed by VanderVeer and Jaluria [2] [2] to solve such a problem.

The present work is the logical progression of the inverse plume in a crossflow problem, the inverse jet in a crossflow problem. The inverse jet in a crossflow problem has many more practical applications and ...

*Corresponding Author
*Email address:* jaluria@soemail.rutgers.edu (Yogesh Jaluria)

**Nomenclature**

| | |
|---|---|
| $\boldsymbol{r}$ | vector location of sampled points |
| $a$ | number of sample locations used in the predictor stage |
| $b, m$ | model parameters |
| $C_1, C_2, C_{1\epsilon}, C_\mu, \sigma_k, \sigma_\epsilon$ | $k-\epsilon$ model coefficients |
| $d$ | number of simulations |
| $E$ | thermal energy |
| $F$ | minimization function |
| $k, \epsilon$ | turbulence kinetic energy, dissipation rate |
| $l, I$ | turbulence length scale and intensity |
| $n$ | number of sample locations |
| $P$ | pressure |
| $P_{rt}$ | turbulent Prandtl number |
| $T$ | temperature |
| $t$ | time |
| $U$ | free stream velocity |
| $X, Y$ | normalized coordinates |
| $x, y$ | coordinates |

**Greek Symbols**

| | |
|---|---|
| $\boldsymbol{\Delta}$ | relative difference between the first sampled point and other sampled points |
| $\boldsymbol{\delta}$ | vector distance between the actual sampled location and the current test location |
| $\lambda$ | thermal conductivity |
| $\mu$ | dynamic viscosity |
| $\mu_t$ | eddy viscosity |
| $\phi$ | normalized temperature $\phi = \frac{T-T_\infty}{T_S-T_\infty}$ |
| $\rho$ | density |
| $\varepsilon$ | error associated with the inverse convection method at a location with given sampled data |

**Superscripts**

| | |
|---|---|
| $*$ | predictor stage, alternative heat flux eqn. |

**Subscripts**

| | |
|---|---|
| $0, 1, 2$ | sample point indexes |
| $\infty$ | free stream |
| $A, B$ | data set A,B |
| $i, j, k$ | index |
| $mod$ | modified |
| $O$ | optimized |
| $P$ | predicted |
| $S$ | source |

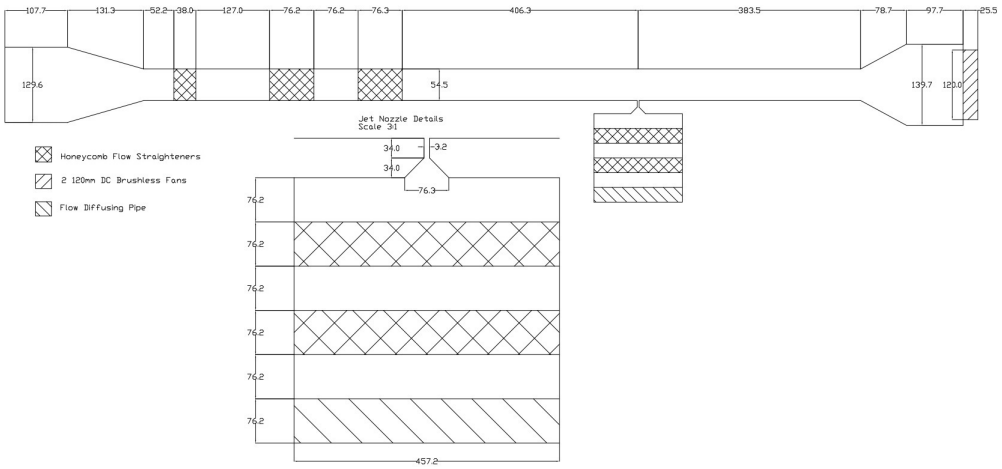


Figure 1: Schematics of the wind tunnel and jet

## 2. Experimental System

The experiment consists of a wind tunnel with a surface level jet located within the test section. The jet uses compressed air passed through flow straighteners to achieve a velocity of $U_S$ and is heated to temperature $T_S$. The jet is subjected to a perpendicular crossflow of velocity $U_\infty$. Figure 1 is a diagram of the wind tunnel and jet, dimensions are in millimeters.

The wind tunnel test section dimensions are $54.5 \times 305 \times 254\,mm$. The maximum velocity of the wind tunnel is $5.0\,m/s$. The jet is heated by electric cartridge heaters (Omega AHP-7561) with a maximum temperature of $425\,K$ due to material limitations of the wind tunnel. The X-direction is directed downstream of the wind tunnel with the zero at the center of the jet. The Y-direction is in the direction of the jet and is zero at the surface of the wind tunnel. Due to the large aspect ratio of the wind tunnel the flow is assumed to be two-dimensional.

The free stream velocity is determined by a Pitot-Static tube attached to a NIST traceable differential pressure sensor from Omega(PX655-0.1DI). The pressure sensor has a full scale reading of 0.1 inches of water and is accurate to 0.05% of full scale. This results in a maximum of 3% error of the calculated velocity.

The jet velocity is determined utilizing a rotameter and verified using a

Pitot-Static tube attached to the same previously described pressure sensor. This results in the same amount of error of 3% for the jet velocity.

The temperature of domain is measured using a K-type thermocouple mounted to an X-Y traversing stage. Sampled data over the course of several days indicate repeatability of the experiment to within 2%.

## 3. Numerical Simulations

The simulations were all performed using Ansys Fluent[3]. The Navier-Stokes equations were solved using a three-dimensional, steady state, realizable $k-\epsilon$ model with enhanced wall effects. Conjugate heat transfer is modelled. The free stream Reynolds number is of order $6 \times 10^3$, while the jet Reynolds number is between $10^3$ and $10^4$. The Rayleigh number is of order $10^7$.

The governing equations are expressed below:

$$u_i = \overline{u_i} + u_i^{'} \tag{1}$$

$$\frac{\partial \rho}{\partial t} + \frac{\partial}{\partial x_i}\left(\rho u_i\right) = 0 \tag{2}$$

$$\begin{aligned} &\frac{\partial}{\partial t}\left(\rho u_i\right) + \frac{\partial}{\partial x_j}\left(\rho u_i u_j\right) = \\ &\qquad \frac{\partial P}{\partial x_i} + \frac{\partial}{\partial x_j}\left[\mu\left(2S_{ij} - \frac{2}{3}\delta_{ij}\frac{\partial u_k}{\partial x_k}\right) - \rho\overline{u_i^{'}u_j^{'}}\right] \end{aligned} \tag{3}$$

$$\begin{aligned} &\frac{\partial}{\partial t}\left(\rho E\right) + \frac{\partial}{\partial x_i}\left[u_i\left(\rho E + P\right)\right] = \\ &\qquad \frac{\partial}{\partial x_i}\left[\left(\lambda + \frac{C_p \mu_t}{P_{rt}}\right)\frac{\partial T}{\partial x_i}\right] \end{aligned} \tag{4}$$

$$\begin{aligned} &\frac{\partial}{\partial t}\left(\rho k\right) + \frac{\partial}{\partial x_j}\left(\rho k u_j\right) = \\ &\qquad \frac{\partial}{\partial x_j}\left[\left(\mu + \frac{\mu_t}{\sigma_k}\right)\frac{\partial k}{\partial x_j}\right] + \frac{\partial u_j}{\partial x_i}\left(-\rho\overline{u_i^{'}u_j^{'}}\right) \\ &\qquad - g_i \frac{\mu_t}{\rho P_{rt}}\frac{\partial \rho}{\partial x_i} + \rho\epsilon \end{aligned} \tag{5}$$

$$\frac{\partial}{\partial t}(\rho\epsilon) + \frac{\partial}{\partial x_j}(\rho\epsilon u_j) = \frac{\partial}{\partial x_j}\left[\left(\mu + \frac{\mu_t}{\sigma_\epsilon}\right)\frac{\partial \epsilon}{\partial x_j}\right] + \rho C_1 S\epsilon - \rho C_2 \frac{\epsilon^2}{k + \sqrt{\nu\epsilon}} - C_{1\epsilon}\frac{\epsilon}{k} C_{3\epsilon} g_i \frac{\mu_t}{\rho P_{rt}}\frac{\partial \rho}{\partial x_i} \tag{6}$$

$$-\rho\overline{u_i' u_j'} = 2\mu_t S_{ij} - \frac{2}{3}\delta_{ij}\left(\rho k + \mu_t \frac{\partial u_k}{\partial x_k}\right) \tag{7}$$

The constants for the turbulence model are [4, 5] :

$$C_{1\epsilon} = 1.44, C_2 = 1.9, \sigma_k = 1.0, \sigma_\epsilon = 1.2, P_{rt} = 0.85 \tag{8}$$

$$C_1 = max\left[0.43, \frac{Sk/\epsilon}{Sk/\epsilon + 5}\right], S = \sqrt{2S_{ij}S_{ji}}, C_{3\epsilon} = tanh\left(\frac{u_g}{u_p}\right) \tag{9}$$

$$\mu_t = \frac{\rho C_\mu k^2}{\epsilon} \tag{10a}$$

$$C_\mu = \frac{1}{A_0 + \frac{A_1 k U^*}{\epsilon}} \tag{10b}$$

$$U^* \equiv \sqrt{S_{ij}S_{ji} + \Omega_{ij}\Omega_{ji}} \tag{10c}$$

$$A_0 = 4.04 \tag{10d}$$

$$A_1 = \sqrt{6} cos\left[\frac{1}{3} cos^{-1}\left(\sqrt{6}\frac{S_{ij}S_{jk}S_{ki}}{(S_{ij}S_{ji})^{\frac{3}{2}}}\right)\right] \tag{10e}$$

$$S_{ij} = \frac{1}{2}\left(\frac{\partial u_i}{\partial x_j} + \frac{\partial u_j}{\partial x_i}\right) \tag{10f}$$

$$\Omega_{ij} = \frac{1}{2}\left(\frac{\partial u_i}{\partial x_j} - \frac{\partial u_j}{\partial x_i}\right) \tag{10g}$$

Where the $u_g$ and $u_p$ are the velocity component parallel and perpendicular to gravity respectively.

The inflow boundary conditions are:

$$u = U_\infty, v = 0, T = T_\infty, P = P_\infty, l = 4mm, I = 5\% \tag{11a}$$

$$k = \frac{3}{2}\left(U_\infty I\right)^2 \tag{11b}$$

$$\epsilon = C_\mu^{3/4}\frac{k^{3/2}}{l} \tag{11c}$$

The jet inflow boundary conditions are:

$$u = 0, v = U_S, T = T_S, P = P_\infty, l = 4mm, I = 5\% \tag{12a}$$

$$k = \frac{3}{2}\left(U_\infty I\right)^2 \tag{12b}$$

$$\epsilon = C_\mu^{3/4}\frac{k^{3/2}}{l} \tag{12c}$$

The upper boundary was taken to be symmetric to reduce the possibility of errors by the experimentally accurate no-slip condition. The upper boundary is very far from the jet and therefore should have negligible effect on the numerical result. The bottom of the wind tunnel is made up of $12\,mm$ thick acrylic, while the test section is $25.4\,mm$ thick acrylic. The external boundary conditions are iso-thermal with a temperature of $T_\infty$. The test section external temperature is iso-thermal of $\frac{1}{2}\left(T_S + T_\infty\right)$. The outflow boundary is a simple pressure outflow of $P_\infty$.

### *3.1. Simulation Validation*

A simulation validation study was performed to verify the results of the simulations. Typical verification was performed including flow model, grid independence, iterative convergence, and lastly comparison with experimental results. The conditions of the simulation validation are shown in table 1.

The results from Spalart-Allmaras, $k-\epsilon$, and $k-\omega$ were compared and the three models have a similar trend. SA tends to be a bit off, but this is expected due to issues with this type of problem[5]. All of the values were normalized utilizing the following equations, where $D$ is the width of the jet.

| Parameter | Value |
|---|---|
| $U_\infty\,(m/s)$ | $2.0 \pm 0.02$ |
| $U_S\,(m/s)$ | $2.0 \pm 0.2$ |
| $T_\infty\,(K)$ | $305 \pm 0.5$ |
| $P_\infty\,(kPa)$ | $101.3 \pm 0.01$ |
| $T_S\,(K)$ | $350 \pm 2.0$ |

Table 1: Validation test conditions

Figure 2 shows a comparison of the flow models at $X = 4.75$.

$$\phi = \frac{T - T_\infty}{T_S - T_\infty} \tag{13a}$$

$$X = \frac{x}{D} \tag{13b}$$

$$Y = \frac{y}{D} \tag{13c}$$

$$V = \frac{U}{U_\infty} \tag{13d}$$

$$V_S = \frac{U_S}{U_\infty} \tag{13e}$$

Grid independence is demonstrated by testing the temperature at a few locations with various grid sizes and geometries, as shown in table 2. Very little variation in simulated temperature over such a wide variety of cell counts shows that the result is most likely grid independent. The grid employed is an unstructured hexagonal mesh with refinement located near the jet and down stream of the jet.

Iterative convergence is typically proven by increasing the residual requirements to very tiny amounts. In this case, due to the extremely small elements within the jet, a residual of $10^{-8}$ was used. Figure 3 is a plot of error compared to the $10^{-8}$ residuals for several residual cases. It can be seen that the error is progressively reducing and a residual of $10^{-6}$ should give acceptable iterative errors (experimental - numerical errors will be much larger).

The final validation is comparing the simulation against the experiment. This is done in figure 4. The simulation matches the experiment closely, with

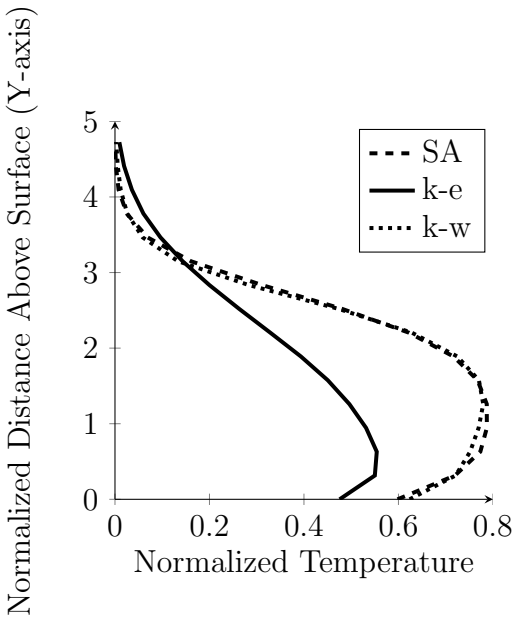


Figure 2: Validation of the simulation: local temperature using three flow models at $X = 4.75$

| Location (x,y) (mm) | 0,1 | 10,5 | 15,5 | 30,10 |
|---|---|---|---|---|
| Cell Count | | | | |
| 57660 | 337.7 | 323.3 | 321.6 | 310.1 |
| 83888 | 337.7 | 323.3 | 321.6 | 310.1 |
| 166352 | 337.7 | 323.2 | 321.5 | 310.1 |
| 366168 | 337.7 | 323.2 | 321.5 | 310.1 |

Table 2: Grid Independence Study, local static temperature (K)

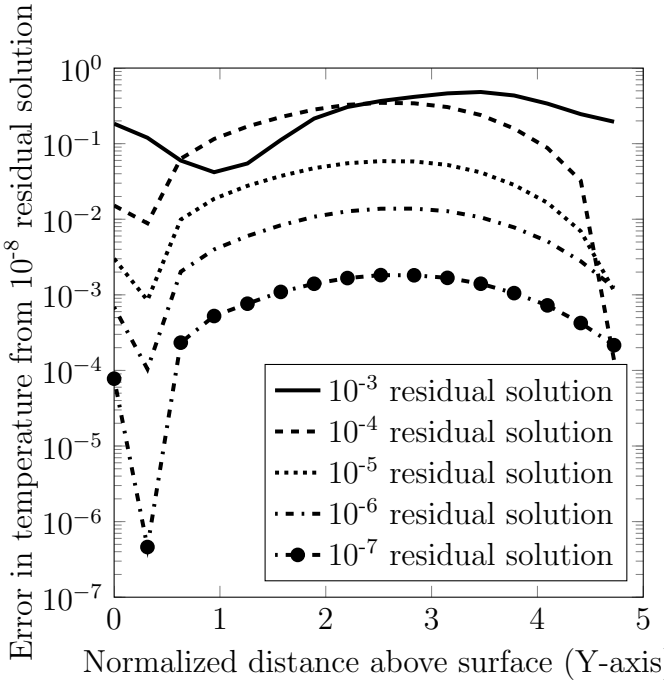


Figure 3: Validation of the simulation: local temperature error vs residuals set to $10^{-8}$ at $X = 4.75$

the exception of very close to the wall.

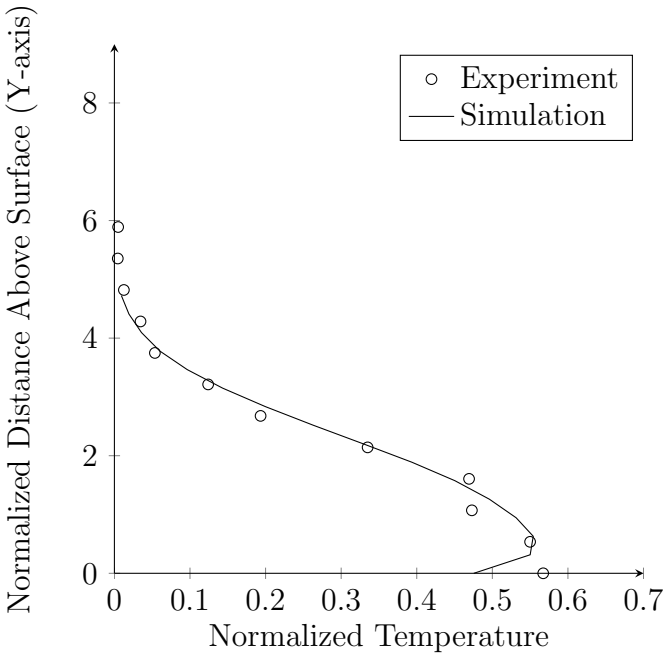


Figure 4: Validation of the simulation: local temperature - experiment versus simulation at $X = 4.75$

## 4. Inverse Solution Methodology

## 5. Results and discussions

## 6. Conclusions

## References

[1] J. Issa, Z. Yin, C. E. Polymeropoulos, Y. Jaluria, Temperature distribution in an optical fiber draw tower furnace, Journal of Materials Processing and Manufacturing Science vol 4 (1996) 221–232.

[2] J. VanderVeer, Y. Jaluria, Solution of an inverse convection problem by a predictor-corrector approach, International Journal of Heat and Mass Transfer vol65 (2013) 123–130.

[3] Ansys, Fluent (version 13), 2010.

[4] T. hsing Shih, W. Liou, A. Shabbir, Z. Yang, J. Zhu, A new $k - \epsilon$ eddy viscosity model for high reynolds number turbulent flows, Computer Fluids vol 24 (1995) 227–238.

[5] Ansys, Fluent Technical Documents v14.0, Technical Report, Ansys, 2011.